Light-mass Bragg cavity polaritons in planar quantum dot lattices

E. M. Kessler,* M. Grochol, and C. Piermarocchi
Department of Physics and Astronomy, Michigan State University, East Lansing, Michigan 48824, USA
(Received 16 October 2007; published 8 February 2008)

The exciton-polariton modes of a quantum dot lattice embedded in a planar optical cavity are theoretically investigated. Umklapp terms, in which an exciton interacts with many cavity modes differing by reciprocal lattice vectors, appear in the Hamiltonian due to the periodicity of the dot lattice. We focus on Bragg polariton modes obtained by tuning the exciton and the cavity modes into resonance at high symmetry points of the Brillouin zone. Depending on the microcavity design, these polariton modes at finite in-plane momentum can be guided and can have long lifetimes. Moreover, their effective mass can be extremely small, of the order of $10^{-8}m_0$ (m_0 is the bare electron mass), and they constitute the lightest excitonlike quasiparticles in solids.

DOI: 10.1103/PhysRevB.77.085306 PACS number(s): 78.20.Bh, 71.36.+c, 78.67.Hc

I. INTRODUCTION

The observation of vacuum Rabi oscillations between a quantum dot (QD) exciton and a cavity photon represents a distinctive example of cavity quantum electrodynamics realized in a solid state system.[1–3] The strong light-matter coupling in networks of cavities and dots is very attractive for the realization of scalable quantum information devices.[4] Furthermore, fundamental investigations on quantum phase transitions in extended cavity systems have recently attracted significant interest.[5–7] The strong light-matter coupling between excitons and photons is often described in terms of polariton modes, which identify propagating electromagnetic modes in a medium with strong dispersive properties. Lately, there has been a considerable theoretical and experimental effort on polariton condensation in planar microcavities.[8–11] In the simplest picture, the critical temperature for polariton condensation is inversely proportional to the polariton effective mass. Given their small effective mass (about 4 orders of magnitude smaller than excitons), quantum well polaritons suggest the possibility of creating a condensate at high temperature. Therefore, it is important to investigate diverse geometrical realizations of polaritonic structures, where the photon and matter excitations are confined in different ways. These diverse geometries could lead both to quantum information devices and to systems in which coherent matter states can be obtained at room temperature.

In this paper, we exploit the recently gained opportunity of growing artificial structures with spatial periodicity comparable to the wavelength of the confined quasiparticle, the exciton in our case, and their embedding in a microcavity. The main idea consists in tuning the exciton energy in such a way that at least two photon modes with different momenta are resonantly coupled to it due to the lattice symmetry. We assume that the exciton-photon coupling is stronger than the exciton inhomogeneous broadening. There has been many proposals for engineering exciton polaritons, or two-level system polaritons, using periodic structures: with periodic quantum well (QW) Bragg structures,[12,13] cavity-free three-dimensional arrays of QDs[14] or two-level atoms,[15] point-dipole crystal,[16] photonic band gaps with antidots,[17] and confined QW polaritons in mesa structures.[18] Overall, two-dimensional polaritonic structures have the advantage that the in-plane momentum can be directly mapped onto an emission angle and the dispersion law can be easily probed. Here, we consider a system with a mismatch between the continuous symmetry of the two-dimensional photons in the cavity and the discrete symmetry of a quantum dot lattice. In the proposed structure, the polariton dispersion is entirely determined by the coupling between the exciton in the dots and two dimensional photons, which leads to in-plane effective masses that can be exceptionally small, of order of $10^{-8}m_0$, for some highly symmetric points in the first Brillouin zone. The group velocity of two-dimensional photons is large for large in-plane momenta. This can be seen as the underlying reason behind such a small polariton mass at the zone edge. The extremely small mass makes this structure a promising candidate for approaches to high temperature polariton condensation and for long-range coupling of spin[19] or exciton[20] qubits.

This paper is organized as follows: In Sec. II, we introduce the system and write the Hamiltonian for the QD lattice interacting with the two-dimensional photon modes. The energy dispersion of the polariton states for some highly symmetric points in the Brillouin zone of the square and hexagonal lattice is presented in Sec. III. In the same section, we also discuss the exciton-light mixing, the effective masses, and the polariton lifetime. Conclusions are found in Sec. IV. In the Appendixes we provide the explicit form of the exciton-photon coupling constant, we discuss an optimization procedure for the system design, and we give the exact effective mass expressions.

II. POLARITON HAMILTONIAN

We consider the system shown in Fig. 1. A two-dimensional lattice of QDs or impurities is placed at the center of a planar cavity structure, i.e., a Fabry-Pérot resonator. There is currently an intense experimental effort for controlling the growth of QDs based on self-assembly and growth on patterned substrates.[21,22] Controlled impurity implantation or micropatterned electrostatic traps on a quantum well[23,24] are further options to realize the proposed structure. We assume that the array consists of identical QDs, and we use the effective mass, envelope function, and single sublevel approximations.[25] Furthermore, taking into account that the

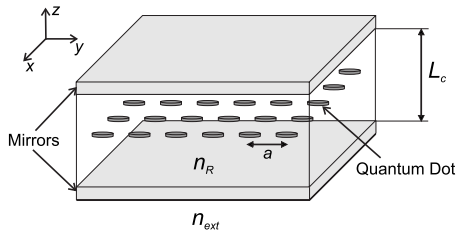

FIG. 1. Scheme of the system studied. An ideal quantum dot lattice is embedded in a planar microcavity of length L_c and refractive index n_R.

confinement potential of a QD can be modeled by a harmonic potential,[26] which enables the center-of-mass and relative motion separation,[27,28] we write the ground state heavy hole exciton wave function in the QD centered at $\mathbf{R}_j$ in the lattice plane as

$$\Psi_j(\mathbf{r}_e,\mathbf{r}_h) = \chi(\mathbf{R}-\mathbf{R}_j)\Phi(\rho)\phi_e(z_e)\phi_h(z_h), \tag{1}$$

where $\phi_{e(h)}(z_{e(h)})$ is the electron (hole) z-confinement wave function, $\Phi(\rho)=\sqrt{2/\pi a_B^2}e^{-\rho/a_B}$ is the exciton relative motion wave function, with a_B being the exciton Bohr radius, and $\chi(\mathbf{R})$ is the exciton center-of-mass wave function

$$\chi(\mathbf{R}) = \sqrt{\frac{2}{\pi\beta^2}}e^{-R^2/\beta^2}, \tag{2}$$

where β is the effective dot radius. By considering only the ground state, we assume that the energy of the first excited state is larger than the exciton-photon coupling, which is of the order of a few meV.

We assume that the photon modes are confined by ideal planar mirrors in a cavity of length L_c, and we consider only the lowest cavity mode with the photon dispersion

$$\hbar\omega_{\mathbf{q}} = \frac{\hbar c}{n_R}\sqrt{q^2+k_z^2}, \tag{3}$$

where c is the speed of light, n_R is the refractive index of the cavity, k_z is fixed to $k_z=\pi/L_c$, and $\mathbf{q}$ is the in-plane momentum. Finally, the in-plane exciton-photon or polariton Hamiltonian in the second quantization reads

$$H = \hbar\omega_x\sum_{j,\mu}\sigma_{j,\mu}^\dagger\sigma_{j,\mu} + \sum_{\mathbf{q},\lambda}\hbar\omega_{\mathbf{q}}a_{\lambda,\mathbf{q}}^\dagger a_{\lambda,\mathbf{q}} + \sum_{j,\mu,\mathbf{q},\lambda}\{g_{j,\mu,\mathbf{q}}^{\lambda *}a_{\lambda,\mathbf{q}}\sigma_{j,\mu}^\dagger + \text{H.c.}\}, \tag{4}$$

where $\hbar\omega_x$ is the exciton energy, $\sigma_{j,\mu}^\dagger$ ($\sigma_{j,\mu}$) is the jth QD exciton creation (annihilation) operator with polarization μ, and $a_{\lambda,\mathbf{q}}^\dagger$ ($a_{\lambda,\mathbf{q}}$) is the photon creation (annihilation) operator for a given polarization λ. The constant $g_{j,\mu,\mathbf{q}}^{\lambda}$ is the exciton-photon coupling constant for the jth QD, which has the property

$$g_{j,\mu,\mathbf{q}}^{\lambda} = e^{i\mathbf{q}\cdot\mathbf{R}_j}g_{0,\mu,\mathbf{q}}^{\lambda}. \tag{5}$$

In the following, we are going to focus on TE cavity modes, and we consider only one exciton polarization. For quantum well polaritons, TM modes give smaller polariton effects due to the weaker light-matter coupling,[29] and we expect the same to be true in the lattice case. The lattice symmetry can be exploited by introducing new exciton operators

$$\sigma_{\mathbf{q}}^\dagger = \frac{1}{\sqrt{N}}\sum_j \sigma_j^\dagger e^{i\mathbf{q}\cdot\mathbf{R}_j}. \tag{6}$$

After some algebra, the polariton Hamiltonian can be written as

$$H = \sum_{\mathbf{q}\in BZ}\left[\hbar\omega_x\sigma_{\mathbf{q}}^\dagger\sigma_{\mathbf{q}} + \sum_{\mathbf{Q}}\hbar\omega_{\mathbf{q}+Q}a_{\mathbf{q}+\mathbf{Q}}^\dagger a_{\mathbf{q}+\mathbf{Q}} + \sum_{\mathbf{Q}}\{g_{\mathbf{q}+\mathbf{Q}}a_{\mathbf{q}+\mathbf{Q}}\sigma_{\mathbf{q}}^\dagger + \text{H.c.}\}\right], \tag{7}$$

where $\mathbf{q}$ is now restricted to the first Brillouin zone (first BZ) due to the periodicity of the QD lattice and $\mathbf{Q}$ is a reciprocal lattice vector. The renormalized coupling constant (omitting polarization indices) $g_{\mathbf{q}}=\sqrt{N}g_{0,\mathbf{q}}$ expressed in terms of materials and structure parameters is given in Appendix A.

Moreover, the light-matter interaction conserves the momentum $\mathbf{q}$ only up to a reciprocal lattice vector. The terms in Eq. (7) involving the exchange of reciprocal lattice vectors are known as exciton Umklapp processes in the literature.[16,30,31] This is in contrast to the QW microcavity case where there is a one-to-one correspondence between cavity and exciton modes (the in-plane momentum is conserved exactly). They can be seen as interband scattering in which a valence electron e_v with momentum $\mathbf{q}_1$ scatters with a photon with momentum $\mathbf{q}_2$ and creates a conduction electron e_c. If the final momentum $\mathbf{q}_1+\mathbf{q}_2$ lies outside the first BZ, then the momentum of the conduction electron is flipped back to the first BZ by adding a reciprocal lattice vector. Since the photon momentum $\mathbf{q}_2$ is not restricted to the first BZ, the Umklapp momentum $\mathbf{Q}$ for excitons can have an arbitrary large magnitude. This is a difference with respect to electron-phonon Umklapp processes,[32] where only the first neighbor reciprocal lattice points are involved.

However, we remark that in Eq. (7) the quantum dot–photon coupling has a structure form factor due to the finite size of the quantum dots, i.e.,

$$g_{\mathbf{q}} \propto e^{-\beta^2 q^2/4}, \tag{8}$$

so that we find a natural cutoff for the reciprocal lattice vectors. Furthermore, in the photonic case, excitonic corrections due to the Coulomb interaction between the conduction electron and the hole left in the valence band have to be included.

For an exciton state with momentum $\mathbf{q}$ away from the zone boundary, many off-resonant Umklapp terms give corrections that do not entail qualitative properties for the polariton quasiparticles. However, the situation can be very different if the structure is built in such a way that the exciton is resonant with the cavity at $\mathbf{q}_0$, which is at or near the BZ boundary. In that case, we can choose, for instance, $\mathbf{Q}_i$ and $\mathbf{Q}_j$ so that the Bragg condition

$$\omega_x \sim \omega_{\mathbf{q}_0-\mathbf{Q}_i} \sim \omega_{\mathbf{q}_0-\mathbf{Q}_j} \tag{9}$$

is satisfied. In general, the number n of reciprocal lattice points satisfying this condition depends on the lattice sym-

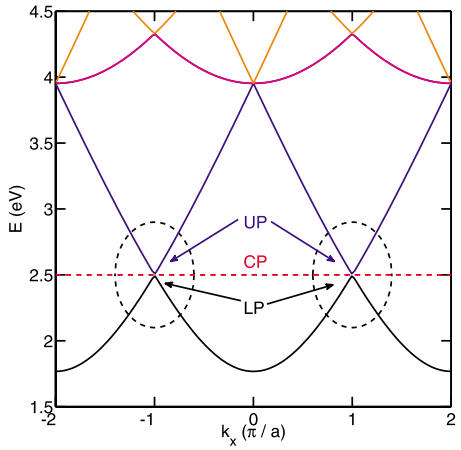

FIG. 2. (Color online) Scheme of photonic branches (solid lines) in a repeated zone scheme. The exciton energy band is indicated by the flat dashed line. Bragg polaritons are obtained by tuning the exciton energy at the zone boundary where photonic branches cross. Upper, lower, and central polariton modes (indicated by UP, LP, and CP) appear due to the light-matter coupling.

metry and on the energy of the exciton. The mode configuration leading to the formation of Bragg cavity polaritons is illustrated in Fig. 2, where the exciton energy (red dashed horizontal line) is tuned in such a way that the polariton mixing occurs at the zone boundary. Due to the reduced symmetry of the dot lattice the $k_z = \pi/L_c$, the cavity mode is folded, giving rise to many photonic branches, each characterized by a different reciprocal lattice vector $\mathbf{Q}$. In order to visualize this folding, the figure shows two repeated BZs. Bragg polariton modes will appear at $\mathbf{q}_0$ where two or more photonic branches are crossing and are nearly degenerate with the exciton energy. These polaritons will have different properties from those of polaritons usually investigated at $\mathbf{q}_0 \sim 0$. Figure 3 shows the high symmetry points at the zone boundary for the square and hexagonal lattices for which we

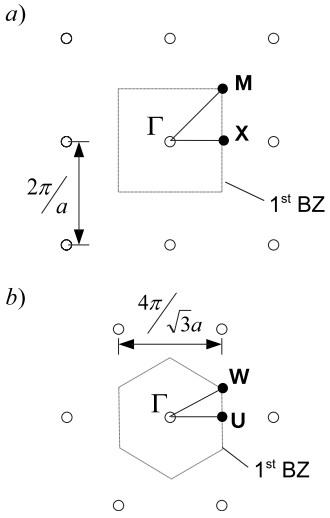

FIG. 3. Reciprocal lattice of a square lattice (a) and of a hexagonal lattice with lattice constant a (b). High symmetry points discussed in the text are indicated.

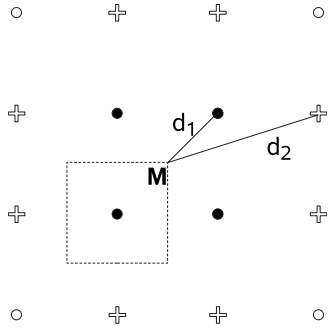

FIG. 4. Bragg resonances at the M point: M_1 labels the energy and momentum of Bragg polaritons obtained with the four nearest neighbor reciprocal lattice points (black dots). M_2 is a higher order Bragg resonance involving eight second nearest neighbor reciprocal lattice points (crosses).

will discuss Bragg polaritons in the following.

Due to the cutoff introduced by the finite quantum dot size, we can write the single polariton Hamiltonian at fixed $\mathbf{q}$ in the form

$$\begin{pmatrix} \hbar\omega_x & g_{\mathbf{q}} & g_{\mathbf{q}+\mathbf{Q}_1} & g_{\mathbf{q}+\mathbf{Q}_2} & \cdots & g_{\mathbf{q}+\mathbf{Q}_{max}} \\ g_{\mathbf{q}} & \hbar\omega_{\mathbf{q}} & 0 & 0 & \cdots & 0 \\ g_{\mathbf{q}+\mathbf{Q}_1} & 0 & \hbar\omega_{\mathbf{q}+\mathbf{Q}_1} & 0 & \cdots & 0 \\ g_{\mathbf{q}+\mathbf{Q}_2} & 0 & 0 & \hbar\omega_{\mathbf{q}+\mathbf{Q}_2} & \cdots & 0 \\ \vdots & \vdots & \vdots & \vdots & \ddots & \vdots \\ g_{\mathbf{q}+\mathbf{Q}_{max}} & 0 & 0 & 0 & \cdots & \hbar\omega_{\mathbf{q}+\mathbf{Q}_{max}} \end{pmatrix}, \tag{10}$$

where the largest reciprocal lattice vector is equal to $|\mathbf{Q}_{max}| \sim 2\pi/\beta$. If we keep only the n resonant terms at the zone boundary, satisfying exactly the Bragg condition, the matrix [Eq. (10)] can be diagonalized analytically, and we find the two eigenvalues

$$\lambda_{1,2} = \hbar\omega_x \pm \sqrt{n} g_{\mathbf{q}} \tag{11}$$

corresponding to the strongly mixed polariton states, as well as the $(n-1)$-fold degenerate eigenvalue

$$\lambda_3 = \hbar\omega_x. \tag{12}$$

The normal mode splitting (Rabi energy), i.e., the difference between the lowest (lower polariton) and the highest (upper polariton) energy at resonance, is then

$$\hbar\Omega = 2\sqrt{n} g_{\mathbf{q}} \tag{13}$$

and is proportional to the square root of the number of reciprocal lattice vectors involved in the Bragg condition.

In the square lattice, we focus on Bragg polaritons obtained at the X and M high symmetry points defined in Fig. 3(a). The number of photonic branches that can be brought into resonance is determined by the number of points in the reciprocal lattice equidistant to X or M, according to Eq. (9). There are two nearest equidistant points to X ($n=2$) and four nearest equidistant points to M ($n=4$) (see dots in Fig. 4). However, if we do not concentrate on the lowest photonic

TABLE I. Number of modes n and parameter ξ for the Bragg polaritons discussed in the text.

	X	M_1	M_2	W
ξ	1	$\sqrt{2}$	$\sqrt{10}$	4/3
n	2	4	8	3

branches and the nearest neighbors in the reciprocal lattice, but, e.g., on the second nearest neighbors, then a larger number of reciprocal lattice vectors can be involved. For instance, there are eight second-nearest-neighbor equidistant points to M ($n=8$, see crosses in Fig. 4). In the following, we will label the M polariton states as M_1 if $n=4$ and M_2 if $n=8$. For the hexagonal lattice [see Fig. 3(b)], we restrict our discussion to the W point which has $n=3$. The U point is similar to the X point of the square lattice and will not be discussed. Since it is possible to express explicitly the coupling constant for a given high symmetry point of length $q_0=\xi\pi/a$ [see Eq. (B3) in Appendix B]. Then the normal mode splitting can be written as

$$\hbar\Omega = 2\frac{\sqrt{n}}{\xi}g_X, \tag{14}$$

where g_X is the coupling constant at the X point. The values of n and ξ can then be used as scaling parameters to calculate the strength of polaritonic effects at different symmetry points, and are summarized in Table I.

Effective mass at X point

One of the most interesting features of Bragg polaritons consists in their extremely small effective mass, which is a consequence of the fact that two-dimensional photons at large momentum enter in the polariton formation. In this section, we investigate this property analytically for a Bragg polariton at the X point. The photon energy in the vicinity of the X point can be expanded to the second order in the in-plane momentum as

$$E_X(q_x,q_y) = \frac{\hbar c}{n_R}\sqrt{k_z^2 + (\pi/a - q_x)^2 + q_y^2}$$
$$\sim E_X^0 + \alpha(-2\pi q_x/a + \nu^2 q_x^2 + q_y^2),$$

where E_X^0 is the X-point photon energy, $\alpha=E_X^0/2K^2$, and $\nu=k_z/K$, with $K=\sqrt{k_z^2+(\pi/a)^2}$. Taking into account only the exciton modes and the two photonic branches nearly resonant in the vicinity of the X point, the full Hamiltonian in the Eq. (10) matrix can be simplified as

$$\begin{pmatrix} 0 & g_X & g_X \\ g_X & \alpha(-2\pi q_x/a + \nu^2 q_x^2 + q_y^2) & 0 \\ g_X & 0 & \alpha(2\pi q_x/a + \nu^2 q_x^2 + q_y^2) \end{pmatrix},$$

where the zero of the energy is set at E_X^0. The eigenvalues of this matrix can be found analytically by solving a cubic equation. From the expansion of the eigenvalues to the second order in q_x and q_y, we obtain

$$\frac{E_{UP(LP)}}{E_X^0} = 1 \pm \sqrt{2}\tilde{g}_X + \frac{1}{4K^2}(q_y^2 + \nu^2 q_x^2) \pm \frac{\sqrt{2}}{4K^2\tilde{g}_X}\left(\frac{\pi}{aK}\right)^2 q_x^2, \tag{15}$$

$$\frac{E_{CP}}{E_X^0} = 1 + \frac{1}{2K^2}(q_y^2 + \nu^2 q_x^2), \tag{16}$$

where the UP CP, and LP index identify the upper, central, and lower polariton branches, respectively. The upper (lower) sign refers to UP (LP), and

$$\tilde{g}_X = \frac{g_X}{E_X^0} \tag{17}$$

is the renormalized coupling constant. From the definition of the effective mass tensor, it follows that for the upper and lower polariton branches,

$$\frac{1}{m_{xx}} = \frac{E_X^0}{2\hbar^2K^2}\left[\nu^2 \pm \frac{\sqrt{2}}{\tilde{g}_X}\left(\frac{\pi}{aK}\right)^2\right],$$

$$\frac{1}{m_{yy}} = \frac{E_X^0}{2\hbar^2K^2}. \tag{18}$$

In these expressions, we have neglected the weak dependence of the coupling constant g_X on the momentum $\mathbf{q}$. This dependence gives small corrections to the effective mass and is discussed in Appendix C. Since, typically, $\tilde{g}_X \sim 10^{-3}$ and $L_c \sim a$, the effective mass ratio reads

$$\frac{m_{xx}}{m_{yy}} = \frac{\tilde{g}_X}{\sqrt{2}}\left(\frac{Ka}{\pi}\right)^2 \sim 10^{-3}. \tag{19}$$

Therefore, the polariton mass is very anisotropic at the X point. We can also compare the value of these effective masses with the QW polariton mass, which is of the same order of magnitude of the cavity photon mass

$$m_{ph} = \frac{\hbar n_R}{c}k_z, \tag{20}$$

and typically $\sim 10^{-5}m_0$. Then, we remark that for the mass along the ΓX direction, we have $m_{xx}/m_{ph} \sim 10^{-3}$ and $m_{yy}/m_{ph} \sim 1$. This implies that a value of the order of $10^{-8}m_0$ is expected. Moreover, we will see in the next section that isotropic masses of such order can be obtained at special high symmetry points.

III. RESULTS AND DISCUSSION

In this section, we present the numerical results for three high symmetry points of the square and hexagonal lattices. The numerical calculations include all resonant and off-resonant terms. We have taken parameters from AlGaAs/GaAs and CdSe/ZnSe systems, which are typical examples of III-V and II-VI quantum dot structures. In general, II-VI semiconductor microcavities have a stronger light-matter coupling; e.g., for CdTe microcavity the light-matter coupling is $g \sim 20$ meV,[33] while for III-V systems the cou-

TABLE II. Optimal values for the lattice constant a as discussed in Appendix B and corresponding polariton splitting energies $\hbar\Omega$ for several high symmetry points for two AlGaAs/GaAs (1) and CdSe/ZnSe (2) systems. The cavity length L_c is 202 and 182 nm for the III–V and the II–VI systems, respectively.

	X	M_1	M_2	W
a_1 (nm)	121	300	383	161
a_2 (nm)	118	167	373	157
$\hbar\Omega_1$ (meV)	2.2	2.2	1.4	2.0
$\hbar\Omega_2$ (meV)	8.8	8.8	5.6	8.0

pling constant is $g \sim 2$ meV.[34] The cavity length, dot size, and lattice constant can be optimized in order to maximize the light-matter coupling for Bragg polaritons at a given high symmetry point. The optimization procedure is discussed in Appendix B, and the parameters are given in Table II.

Figures 5(a)–5(d) show contour plots of the energy dispersion of the upper polariton branch for Bragg polaritons at the X point (a), M point [(b) for M_1 polariton and c for M_2 polariton] of the square lattice, and W point (d) of the hexagonal lattice. The energy dispersion near the resonance reflects the symmetry of these points. We can also see that the polariton effective mass is highly anisotropic for the X polariton, as discussed in the previous section, while the effective mass for M_2 is almost isotropic. In Fig. 6, we show the energy dispersion of the Bragg polariton modes for X polaritons, M_1 polaritons, and W polaritons. The different behaviors of the UP, CP, and LP modes at different points shows how richer Bragg polaritons are compared to the QW polaritons. Note that the total number of branches crossing or anticrossing at the different symmetry points is always given by $n+1$.

At the X point, we have $n=2$; consequently, there are three polariton modes. In the q_y direction, the upper and lower X polaritons are similar to the QW polariton [see Fig. 6(b)]. However, there is one additional central mode degenerate with the photon mode along the zone boundary in the q_y direction. On the contrary, the q_x dependence along $\overline{\Gamma X}$ shows the existence of (i) a lower branch with a negative effective mass in one direction, (ii) an upper branch with positive effective masses but high anisotropy, and (iii) a flat branch with a large mass (consequence of the infinite exciton mass considered in our model) with energy exactly between the lower and upper branches.

Let us now look at the M_1 polaritons, which have five branches. In the $q_x=q_y$ direction, we can see nearly flat photonic branches originating from photon modes with $\mathbf{Q}=(2\pi/a,0)$ and $\mathbf{Q}=(0,2\pi/a)$, while the polariton mixing occurs mainly with photon modes having $\mathbf{Q}=(0,0)$ and $\mathbf{Q}=(2\pi/a,2\pi/a)$. A similar plot for M_2 (not shown) gives nine polariton branches. Notice that there is not a saddle point at the M point. A polariton mode with isotropic negative mass (lower branch) can give rise to an effective negative index of refraction.[35] In the W-point case, there are four branches and the properties are similar to those of the M point of the square lattice.

In the case of QW polaritons, the excitonic component is equally shared between lower and upper polaritons at the anticrossing. This is also true for the excitonic component in the X point, as shown in Figs. 7(a) and 7(c). At the anticrossing, the UP and LP branches consist of *half excitons;* and consequently, the excitonic component is completely absent in the CP branch. Nevertheless, it increases rapidly away from the anticrossing region. This exciton-photon character swap is a characteristic of the Bragg polaritons since in all the cases investigated we have found analytically and numerically that the excitonic component is always equally shared between the lower and upper polaritons at the anticrossing, the rest being purely photonic.

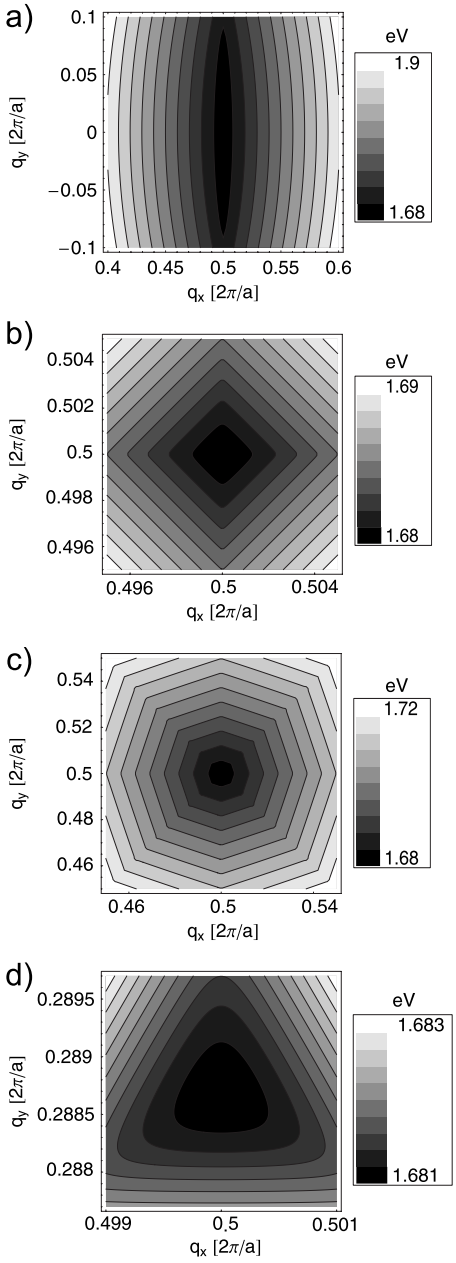

FIG. 5. Contour plot of the upper polariton dispersion at the X point (a), M point [M_1 in (b) and M_2 in (c)], and W point (d). Note the mass anisotropy in the X-point case.

The effective masses calculated numerically for the two material systems are given in Table III. As expected, a strong

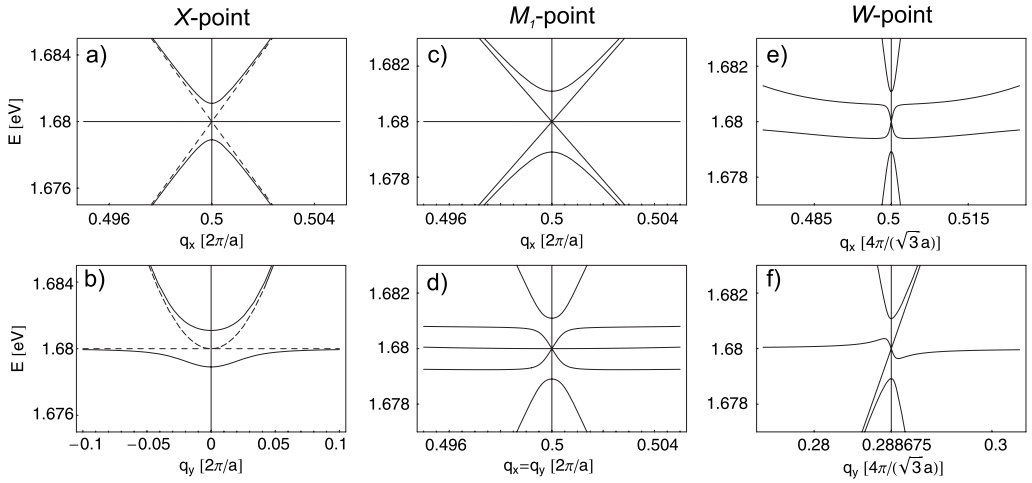

FIG. 6. The energy dispersion of the Bragg polaritons at selected high symmetry points. X polaritons along $\Gamma\bar{X}$ (a) and along $X\bar{M}$ (b), M_1 polaritons along $\Gamma\bar{M}$ (c) and the $q_x=q_y$ axis (d), and W polaritons along the q_x axis (e) and the q_y axis (f). The dashed lines in (a) and (b) represent the uncoupled exciton and photon modes.

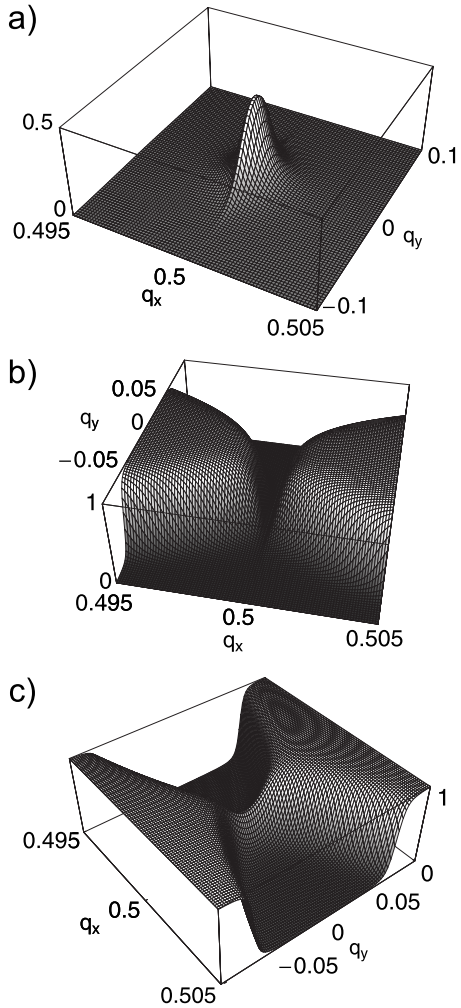

FIG. 7. The exciton component of the lower (a), central (flat) (b), and upper (c) Bragg polaritons at the X point.

anisotropy at the X point and an almost isotropic mass at the M_2 point are found. The numerical values for the X point are the same as those calculated using the analytical formula of Eq. (18), thus validating our numerical approach. Furthermore, the ratio in Eq. (19) for both AlGaAs/GaAs and CdSe/ZnSe systems, for which $\tilde{g}_X \sim 10^{-3}$ and $\tilde{g}_X \sim 10^{-2}$, respectively (see Appendix B for material parameters) is also obtained. The value of the effective mass in some cases is of the order of $10^{-8}m_0$ and thus is extremely small for a matter like quasiparticles. As discussed in the Introduction, the small effective mass could suggest strategies for the realization of polariton condensation in microcavities. However, the dynamics of Bragg polaritons, including the phonon bottleneck effects[36] and polariton-polariton scattering, is expected to be different from that of quantum well polaritons and needs further investigations. The small polariton effective mass can play an important role also in quantum information implementations. It has been recently shown that QW polaritons can mediate a spin-spin coupling between two charged dots or impurities over a distance of the order of hundreds of nanometers due to the light mass of polaritons.[19] Since Bragg polariton states have effective masses that are 2–3 orders of magnitude smaller, the range of the spin coupling could be further extended.

TABLE III. Lower (LP) and upper (UP) polariton effective masses m_{xx} and m_{yy} at X and M_2 points for two systems in units of $10^{-5}m_0$. For comparison, the cavity photon mass $m_{ph}=\hbar n_R k_z/c$ for the two systems are $2.1\times10^{-5}m_0$ and $1.7\times10^{-5}m_0$.

	GaAs/AlGaAs		CdSe/ZnSe	
	X	M_2	X	M_2
m_{xx}^{UP}	3.7×10^{-3}	4.7×10^{-3}	8.0×10^{-3}	1.0×10^{-2}
m_{yy}^{UP}	8.3	4.7×10^{-3}	6.2	1.0×10^{-2}
m_{xx}^{LP}	-3.7×10^{-3}	-4.7×10^{-3}	-8.0×10^{-3}	-1.0×10^{-2}
m_{yy}^{LP}	8.3	-4.7×10^{-3}	6.1	-1.0×10^{-2}

So far, the lifetime of Bragg polaritons has not been discussed. There is an essential difference with respect to the QW polariton case, where the light-matter mixing occurs close to $q=0$. The quantum well polariton lifetime depends on the photon lifetime in the cavity, which is determined by the reflectance of the mirrors in the normal direction and is of the order of picoseconds. However, at finite $\mathbf{q}$, depending on the external index of refraction and on the propagation angle $\theta_p=\arccos\left(\frac{k_z}{K}\right)$, a cavity photon can either be transmitted through the mirrors, or it can remain confined due to total internal reflection. This means that structures can be engineered where the polariton mixing occurs at large $\mathbf{q}$ with *guided* modes, which is never possible in the quantum well case. Since guided photons have, in principle, a much longer lifetime, the polariton lifetime will also be much longer, likely in the order of micro-or milliseconds, depending on the properties of the lateral surfaces of the cavity structures. However, the details of the cavity modes at large in-plane momentum, particularly leaky modes[37] due to the distributed Bragg mirrors, need to be carefully taken into account since they will affect both the dynamics and the radiative properties of these polaritons.

Inhomogeneities in the quantum dot system are expected to affect the results presented so far. If the light-matter interaction is not very strong, Bragg polaritons are sensitive to three kinds of inhomogeneities: energy and oscillator strength fluctuations, and fluctuations in the position due to the deviations from an ideal lattice. We are currently investigating the role of these three kinds of disorder, which affect Bragg polaritons in very different ways.[38]

IV. CONCLUSIONS AND OUTLOOK

We have investigated polariton modes in a planar quantum dot lattice embedded in a microcavity. Assuming small exciton and photon homogeneous broadening, we have considered systems in the strong coupling regime. We have studied Bragg polariton modes formed at high symmetry points of the Brillouin zone. Truly polaritonic quasiparticles with a 50-50 light-matter character appear at these points in upper and lower branches. Analytical and numerical calculations of the polariton effective masses give extremely small values, of the order of $10^{-8}m_0$, and, in some cases, strong anisotropy. The small mass is due to the mixing of excitons with nearly linear two-dimensional photon modes at large momenta. There is a full transfer of the excitonic wave function component from the flat exciton dispersion to photonic branches in the strong coupling region. We have also discussed the possibility of polariton coupling with guided modes, which could lead to a long polariton lifetime.

Future extensions of this work could include (i) an explicit theoretical treatment of the homogeneous broadening with a discussion of the strong to weak coupling transition, (ii) realistic structure modeling of the distributed Bragg mirrors with leaky modes, which could be close to the Bragg polariton resonances, and (iii) sensitivity to inhomogeneous broadening effects. The polariton-phonon, polariton-polariton, and polariton-spin dynamics for these Bragg quasiparticles also need further investigation since they are expected to be very different from those in the quantum well case.

ACKNOWLEDGMENT

This research was supported by the National Science Foundation, Grant No. DMR-0608501.

APPENDIX A: COUPLING CONSTANT

The lattice exciton-photon coupling in the cavity for the TE mode reads[29]

$$g_{\mathbf{q}}^{TE}=ie\omega_x\sqrt{\frac{\hbar}{\epsilon_0 n_R^2\omega_{\mathbf{q}}V}}u_{cv}\sqrt{N}\Phi_{1s}(0)\tilde{\chi}(\mathbf{q})F(L_c), \quad \text{(A1)}$$

where $V=SL_c$ is the volume of the cavity, S being the surface of the cavity, u_{cv} is the dipole matrix element between conduction and valence bands, N is the number of dots in the cavity, $\tilde{\chi}(\mathbf{q})$ is the center-of-mass form factor,

$$\tilde{\chi}(\mathbf{q})=\sqrt{2\pi}\beta e^{-\mathbf{q}^2\beta^2/4},$$

and $F(L_c)$ is the z-form factor

$$F(L_c)=\int dz\phi_e(z)\phi_h(z)\cos\left(\frac{\pi z}{L_c}\right).$$

We can assume that the QW that contains the quantum dots is much narrower than the cavity length L_c, which implies $F(L_c)\sim 1$. The coupling constant for TM modes,

$$g_{\mathbf{q}}^{TM}=\frac{-ik_z}{\sqrt{q^2+k_z^2}}g_{\mathbf{q}}^{TE}, \quad \text{(A2)}$$

is always smaller than that for TE modes at finite in-plane momentum. We can relate the QD coupling constant in Eq. (A1) to the equivalent quantity in the QW case as

$$g_{\mathbf{q}}^{TE}=\frac{\hbar\omega_x}{\hbar\omega_x^{QW}}\sqrt{n_D}\tilde{\chi}_0(\mathbf{q})\frac{a_B^{QW}}{a_B^{QD}}g_{QW}^{TE}, \quad \text{(A3)}$$

where $\hbar\omega_x^{QW}$ is a QW exciton energy, $n_D=N/S_c$ is the QD density, and a_B^{QW} (a_B^{QD}) is a Bohr radius of the QW (QD) exciton. We note that recent numerical calculations show that for confined excitons, the effective Bohr radius defined by the ansatz of Eq. (1) is typically smaller that the quantum well value.[39,40] The quantity $n_{QD}2\pi\beta^2$ can be understood as a filling or packing factor. For a fixed dot size and exciton energy, the hexagonal lattice has the largest packing factor and the largest coupling at $\mathbf{q}=0$. The value of the interband matrix element can be calculated conveniently from the Kane energy parameter using the relation[41]

$$u_{cv}^2=\frac{\hbar^2e^2}{(\hbar\omega_x^{QW})^2}\frac{E_P}{2m_0}. \quad \text{(A4)}$$

TABLE IV. Materials parameters used in the numerical calculations.

	GaAs/AlGaAs	CdSe/ZnSe
$\hbar\omega_x$ (eV)	1.68[a]	2.50[b]
$\hbar\omega_x^{QW}$ (eV)	1.6	2.4
a_B^{QD} (nm)	11	3
a_B^{QW} (nm)	13	6
g_{QW} (meV)	1.2[c]	2.7
n_R	3.5[d]	2.5[d]
E_P (eV)	23[e]	21[f]
β (nm)	35	35
L_{DBR} (μm)	2.0	2.0

[a]Reference 43.
[b]Reference 44.
[c]Comparable with the value found in Ref. 45.
[d]Reference 46.
[e]Reference 25.
[f]Reference 47.

In order to have a strong light-matter coupling, a system with a large dipole matrix element and with a small QD Bohr radius is desired. From this point of view, II-VI semiconductors are better candidates than III-V. Our scheme could also be implemented with impurity-bound excitons, which usually have very strong oscillator strength, large spatial extension, and very small inhomogeneous broadening.[42] The material parameters used in the calculations are given in Table IV.

APPENDIX B: PARAMETER OPTIMIZATION

Let us now fix the QD size and ground state exciton energy. The lattice constant a and cavity length L_c are then adjustable parameters that can be optimized to increase the polariton mixing. The coupling constant at a high symmetry point with $q_0=\xi\frac{\pi}{a}$ can be written as

$$g_{q_0}(a,L_c,\xi)=\frac{1}{\sqrt{L_c+L_{DBR}}}\frac{\beta}{a}e^{-\beta^2\xi^2\pi^2/4a^2}g_c, \tag{B1}$$

where g_c is a constant that does not depend on β, a, and L_c. Note that the dependence on the lattice constant a is nonmonotonic due to the competition between the quantum dot density and the structure factor. Moreover, the exciton-photon Bragg resonance condition gives the constraint

$$\hbar\omega_x=\frac{\hbar c}{n_R}\sqrt{\left(\frac{\xi\pi}{a}\right)^2+\left(\frac{\pi}{L_c}\right)^2}. \tag{B2}$$

In order to take into account that distributed Bragg reflectors are typically used as mirrors, we have added an effective L_{DBR} to the nominal cavity spacer length L_c in the coupling constant.[34] By expressing L_c as a function of a from Eq. (B2), the coupling constant becomes a function of only one variable, $g_{q_0}(a)$. The optimal lattice spacing can then be found by analytical or numerical maximization. Defining $a'=a/\xi$, we obtain the following from Eq. (B1):

$$g_{q_0}(a,L_c,\xi)=\xi^{-1}g_{q_0}(a',L_c,1). \tag{B3}$$

Thus, one needs to optimize a only for one high symmetry point of each material combination and then rescale it by ξ for other points.

APPENDIX C: EFFECTIVE MASS CORRECTIONS

Here, we include the corrections to the effective mass due to the dependence of the coupling constant on $\mathbf{q}$. This provides the exact second order expansion in q_x and q_y of Bragg polaritons and, therefore, the exact expression for their effective mass tensor. Only $g_{\mathbf{q}}^{TE}\equiv g_X$ close to the X point is considered here. The coupling constant written as a function of small $\mathbf{q}$ around the X point reads

$$g_X(q_x,q_y)=g_X^0\frac{e^{-(2\pi q_x/a+q_x^2+q_y^2)\beta^2/4}}{\sqrt[4]{1+(2\pi q_x/a+q_x^2+q_y^2)/K^2}}.$$

Using $(1+x)^{-1/4}=1-\frac{1}{4}x+\frac{5}{32}x^2+O(x^3)$ and the expansion of the exponential function, we obtain

$$g_X(q_x,q_y)=g_X^0+g_X^{1,x}\frac{q_x}{K}+g_X^{2,x}\left(\frac{q_x}{K}\right)^2+g_X^{2,y}\left(\frac{q_y}{K}\right)^2,$$

where

$$g_X^{1,x}=-g_X^0\frac{\pi}{2a}\left(\frac{1}{K}+K\beta^2\right),$$

$$g_X^{2,x}=g_X^0\left[-\frac{1}{4}(1+K^2\beta^2)+\frac{5}{8}\left(\frac{\pi}{Ka}\right)^2\right],$$

$$g_X^{2,y}=g_X^0\left[-\frac{1}{4}(1+K^2\beta^2)\right].$$

The exact expansion for the polaritonic modes is therefore

$$\frac{E_{UP(LP)}}{E_X^0}=1\pm\sqrt{2}\tilde{g}_X^0+\left[\frac{1}{4}\pm\sqrt{2}\tilde{g}_X^{2,y}\right]\left(\frac{q_y}{K}\right)^2+\left[\left(\frac{\nu}{2}\right)^2\pm\frac{1}{2\sqrt{2}\tilde{g}_X^0}\left(\frac{\pi}{Ka}\right)^2\pm\sqrt{2}\tilde{g}_X^{2,x}\mp\frac{1}{\sqrt{2}}\frac{(\tilde{g}_X^{1,x})^2}{\tilde{g}_X^0}-\frac{g_X^{1,x}}{g_X^0}\frac{2\pi}{Ka}\right]\left(\frac{q_x}{K}\right)^2,$$

$$\frac{E_{CP}}{E_X^0}=1+\frac{1}{2}\left[\nu^2+\frac{g_X^{1,x}}{g_X^0}\frac{4\pi}{Ka}\right]\left(\frac{q_x}{K}\right)^2+\frac{1}{2}\left(\frac{q_y}{K}\right)^2. \tag{C1}$$

The effective masses for UP(LP) can be written as

$$\frac{1}{m_{xx}}=\frac{E_X^0}{\hbar^2K^2}\left[\frac{\nu^2}{2}\pm\frac{1}{\sqrt{2}\tilde{g}_X^0}\left(\frac{\pi}{Ka}\right)^2\pm\sqrt{8}\tilde{g}_X^{2,x}\mp\sqrt{2}\frac{(\tilde{g}_X^{1,x})^2}{\tilde{g}_X^0}\pm\frac{g_X^{1,x}}{g_X^0}\frac{4\pi}{Ka}\right],$$

$$\frac{1}{m_{yy}} = \frac{E_X^0}{\hbar^2 K^2}\left(\frac{1}{2} \pm \sqrt{8}\tilde{g}_X^{2,y}\right), \tag{C2}$$

while for CP we have

$$\frac{1}{m_{xx}} = \frac{E_X^0}{2\hbar^2 K^2}\left[\nu^2 + \frac{g_X^{1,x}}{g_X^0}\frac{4\pi}{Ka}\right],$$

$$\frac{1}{m_{yy}} = \frac{E_X^0}{2\hbar^2 K^2}. \tag{C3}$$

The upper and lower polariton small masses in the x direction is mainly due to the $O(1/\tilde{g}_0)$ term, and the $\mathbf{q}$ dependence of the coupling constant provides only small corrections. The numerical calculations of the effective mass given in Table III include the explicit dependence of the coupling constant on the wave vector.

*Present address: Max-Planck Institute for Quantum Optics, Garching, Germany.

[1] J. P. Reithmaier, G. Sęk, A. Löffler, S. K. C. Hofmann, S. Reitzenstein, L. V. Keldysh, V. D. Kulakovskii, T. L. Reinecke, and A. Forchel, Nature (London) **432**, 197 (2004).

[2] T. Yoshie, A. Scherer, J. Hendrickson, G. Khitrova, H. M. Gibbs, G. Rupper, C. Ell, O. B. Shchekin, and D. G. Deppe, Nature (London) **432**, 200 (2004).

[3] E. Peter, P. Senellart, D. Martrou, A. Lemaitre, J. Hours, J. M. Gérard, and J. Bloch, Phys. Rev. Lett. **95**, 067401 (2005).

[4] W. Yao, R. B. Liu, and L. J. Sham, Phys. Rev. Lett. **95**, 030504 (2005).

[5] M. J. Hartmann, F. G. S. L. Brandão, and M. Plenio, Nat. Phys. **2**, 849 (2006).

[6] M. J. Hartmann and M. B. Plenio, Phys. Rev. Lett. **99**, 103601 (2007).

[7] A. D. Greentree, C. Tahan, J. H. Cole, and L. C. L. Hollenberg, Nat. Phys. **2**, 856 (2006).

[8] H. Deng, G. Weihs, D. Snoke, J. Bloch, and Y. Yamamoto, Proc. Natl. Acad. Sci. U.S.A. **100**, 15318 (2003).

[9] J. Kasprzak *et al.*, Nature (London) **443**, 409 (2006).

[10] R. Balili, V. Hartwell, D. Snoke, L. Pfeiffer, and K. West, Science **316**, 1007 (2007).

[11] J. Keeling, F. M. Marchetti, M. H. Szymanska, and P. B. Littlewood, Semicond. Sci. Technol. **22**, R1 (2007), and references therein.

[12] A. V. Mintsev, L. V. Butov, C. Ell, S. Mosor, G. Khitrova, and H. M. Gibbs, JETP Lett. **76**, 637 (2002).

[13] G. R. Hayes, J. L. Staehli, U. Oesterle, B. Deveaud, R. T. Phillips, and C. Ciuti, Phys. Rev. Lett. **83**, 2837 (1999).

[14] E. L. Ivchenko, Y. Fu, and M. Willander, Phys. Solid State **42**, 1756 (2000).

[15] Y. D. Chong, D. E. Pritchard, and M. Soljačić, Phys. Rev. B **75**, 235124 (2007).

[16] K. Kempa, R. Ruppin, and J. B. Pendry, Phys. Rev. B **72**, 205103 (2005).

[17] D. Gerace and L. C. Andreani, Phys. Rev. B **75**, 235325 (2007).

[18] R. I. Kaitouni *et al.*, Phys. Rev. B **74**, 155311 (2006).

[19] G. F. Quinteiro, J. Fernández-Rossier, and C. Piermarocchi, Phys. Rev. Lett. **97**, 097401 (2006).

[20] G. Tarel, G. Parascandolo, and V. Savona, arXiv:0708.1920 (unpublished).

[21] S. Watanabe, E. Pelucchi, K. Leifer, A. Malko, B. Dwir, and E. Kapon, Appl. Phys. Lett. **86**, 243105 (2005).

[22] A. Badolato and P. M. Petroff (unpublished).

[23] A. Gärtner, L. Prechtel, D. Schuh, A. W. Hilleitner, and J. P. Kotthaus, Phys. Rev. B **76**, 085304 (2007).

[24] C. W. Lai *et al.*, Nature (London) **450**, 529 (2007).

[25] G. Bastard, *Wave Mechanics Applied to Semiconductor Heterostructures* (Les éditions de physique, Paris, 1992).

[26] A. Kumar, S. E. Laux, and F. Stern, Phys. Rev. B **42**, 5166 (1990).

[27] M. Sugawara, Phys. Rev. B **51**, 10743 (1995).

[28] M. Sugawara, Jpn. J. Appl. Phys., Part 1 **36**, 2151 (1997).

[29] V. Savona, C. Piermarocchi, A. Quattropani, P. Schwendimann, and F. Tassone, Phase Transitions **68**, 169 (1999).

[30] R. K. Bullough and V. B. Thompson, J. Phys. C **3**, 1780 (1970).

[31] J. Knoester and S. Mukamel, J. Chem. Phys. **91**, 989 (1989).

[32] N. W. Ashcroft and N. D. Mermin, *Solid State Physics* (Brooks/Cole, Thomson Learning, Cornell, 1976).

[33] R. André, D. Heger, L. S. Dang, and Y. M. dAubigne, J. Cryst. Growth **185**, 758 (1998).

[34] V. Savona, L. C. Andreani, P. Schwendimann, and A. Quattropani, Solid State Commun. **93**, 733 (1995).

[35] V. M. Agranovich and Y. N. Gartstein, Phys. Usp. **49**, 1029 (2006).

[36] F. Tassone, C. Piermarocchi, V. Savona, A. Quattropani, and P. Schwendimann, Phys. Rev. B **56**, 7554 (1997).

[37] F. Tassone, C. Piermarocchi, V. Savona, A. Quattropani, and P. Schwendimann, Phys. Rev. B **53**, R7642 (1996).

[38] M. Grochol and C. Piermarocchi (unpublished).

[39] M. Grochol, F. Grosse, and R. Zimmermann, J. Lumin. **112**, 208 (2005).

[40] M. Grochol, F. Grosse, and R. Zimmermann, Phys. Rev. B **71**, 125339 (2005).

[41] E. Rosencher and B. Vinter, *Optoelectronics* (Cambridge University Press, Cambridge, 2002).

[42] B. Stébé, E. Assaid, S. L. Goff, and F. Dujardin, Solid State Commun. **100**, 217 (1996).

[43] D. Gammon, E. S. Snow, B. V. Shanabrook, D. S. Katzer, and D. Park, Phys. Rev. Lett. **76**, 3005 (1996).

[44] I.-C. Robin, R. André, and J.-M. Gérard, Phys. Rev. B **74**, 155318 (2006).

[45] P. Borri, J. R. Jensen, W. Langbein, and J. M. Hvam, Phys. Status Solidi B **221**, 143 (2000).

[46] O. Madelung, *Semiconductors: Data Handbook* (Springer, New York, 2003).

[47] M. Cardona, J. Phys. Chem. Solids **24**, 1543 (1963).